

Failure Properties and Stability Monitoring of Strip and Column Cemented Gangue Backfill Bodies Under Uniaxial Compression In Constructional Backfill Mining

Hongyu Ran

Taiyuan University of Technology

Yuxia Guo (✉ gyx771221@163.com)

Taiyuan University of Technology

Guorui Feng

Taiyuan University of Technology

Chunqing Li

RMIT University

Research Article

Keywords: constructional backfill mining, cemented gangue backfill body, strip, column, length-height ratio, failure properties, stability monitoring

Posted Date: January 3rd, 2022

DOI: <https://doi.org/10.21203/rs.3.rs-1120748/v1>

License:  This work is licensed under a Creative Commons Attribution 4.0 International License. [Read Full License](#)

Version of Record: A version of this preprint was published at Environmental Science and Pollution Research on March 4th, 2022. See the published version at <https://doi.org/10.1007/s11356-022-19336-2>.

Abstract

The strip and column cemented gangue backfill bodies (CGBBs) are the main supporting components in the design of constructional backfill mining for coal mining, which determines the stability of goaf. Previous researches have mostly focused on the mechanical properties of column CGBB, but the mechanical properties of strip CGBB are still unclear. Herein, the uniaxial compression experiments for strip and column CGBBs were conducted to compare the failure properties. The acoustic emission (AE) and two types of resistivity monitoring were used to monitor the damage evolution. The effect of the length-height ratio on the mechanical characteristic of strip CGBB was analyzed by discrete element simulation. The results show that: the strength and peak strain of strip CGBB under uniaxial compression is higher than those of column CGBB, and the strip CGBB shows better ductility. The stress of column CGBB decreases significantly faster than that of strip CGBB at the post-peak stage. The strength and ductility of strip CGBB increase with the increase of length-height ratio. The strip CGBB is destroyed from both ends to the middle under uniaxial compression, and the core bearing area is reduced correspondingly. The AE signal evolution of CGBBs under uniaxial compression before the peak stress contains three stages, and the AE signals of strip CGBB at the peak stress will not rise sharply compared with column CGBB. The resistivity monitoring effect of the horizontally symmetrical conductive mesh is better than that of the axial. The horizontal resistivity increases gradually with the increase of stress under uniaxial compression, and increases sharply at the peak stress, and then drops after the peak stress. The damage constitutive models and the stability monitoring models of the CGBBs are established based on the experimental results. This work would be instructive for the design and stability monitoring of CGBB.

1. Introduction

Coal mining has caused many environmental issues, for instance, surface subsidence, the destruction of underground water and surface ecosystem (Chen et al. 2016), and the pollution problems caused by coal gangue waste (Yang et al. 2021). Moreover, shallow coal resources are gradually depleted, and thus the coal enterprises have to mine the coal resources in the deep (Zhang et al. 2019) and under the water, construction, and railway, which may cause more serious environmental problems (Feng et al. 2020). Generally, the cemented gangue backfill body (CGBB) that was made of coal gangue, cement, fly ash, and water was used to backfill the goaf, which can solve these problems (Zhang et al. 2007; Zhu et al. 2019; Zhang et al. 2017). After the hydration of cement, the hardened CGBB can support the overlying strata. However, the cost of cement is relatively high and the limited raw material coal gangue only accounts for 15-20% of raw coal (Liu et al. 2020). If all the mined-out area is filled with CGBB, the total cost of backfill mining will be very high and the economic efficiency of coal enterprises will deteriorate. Therefore, the constructional backfill mining method was proposed, as shown in Fig. 1, strip and column CGBBs are arranged at key locations in the mined-out area to support the roof (Du et al. 2019a; Du et al. 2019b; Zhu et al. 2017; Zhu et al. 2020; Feng et al. 2019). This method can effectively reduce the cost and achieve the control of roof subsidence, in the meantime, the constructed underground space can be used for other purposes, such as the storage of water resources (Du et al. 2019c; Xu et al. 2015).

As the supporting components for constructional backfill mining, the stability of strip and column CGBBs under the axial compression determines the stability of the goaf and the safety of mining. A series of researches have been carried out on the deformation and failure characteristics of the CGBB sample. The failure characteristics and load-bearing mechanism of large-sized column CGBB under uniaxial compression were studied by experiments (Du et al. 2019a; Du et al. 2019b). The mechanical properties of the combined system of sandstone roof and backfill body were studied, and it found that the strength and elastic modulus of the combined body is between a single backfill body and a single sandstone (Chen et al. 2020). The local deformation characteristics of the CGBB under uniaxial compression and the creep behavior under disturbance conditions were studied (Sun et al. 2018a; Sun et al. 2019). They found that the peak strain of the backfill body was very large, showing multiple shear deformation areas, and the disturbance increases the creep deformation, and the creep instability time is shortened. In addition, the relationship between the strength of the CGBB and the ultrasonic pulse velocity was studied, and a prediction model of the strength and the ultrasonic pulse velocity was established (Wu et al. 2020). The effect of stress curing conditions on the deformation and strength characteristics of the CGBB was studied, which proves that curing stress can increase the strength of the backfill body (Guo et al. 2020). The effect of the particle size distribution of aggregates on the mesoscopic structural evolution of cemented waste rock backfill was studied (Wu et al. 2021a). The creep characteristics of the CGBB under high-stress levels and the lateral creep properties of the cylinder CGBB sample under step-by-step loading were investigated through experiments (Ran et al. 2021; Guo et al. 2021a). Furthermore, to predict creep deformation and creep failure, different scholars have proposed different creep constitutive models for the CGBB (Wu et al. 2021b; Hou et al. 2020). It can be summarized from these studies that the existing experiments mostly used cylindrical or cubic specimens for testing. In practical backfill mining engineering, however, the strip CGBB has been more widely used in coal mining (Xu et al. 2007; Wang et al. 2018; Sun et al. 2018b) and it is essential to ensure the stability of the goaf in constructional backfill mining (Feng et al. 2019). Unfortunately, the damage evolution and failure characteristics of strip CGBB are far from clear. Therefore, comparing and analyzing the deformation and instability characteristics of strip and column CGBBs under axial compression are desired to achieve excellent design of the support components in constructional backfill mining.

Based on the analysis and research of the acoustic emission (AE) signal (Guo et al. 2021b; Xu et al. 2016) and resistivity (Liu et al. 2019) during the compression process of the CGBB, the evolution of the crack system inside the CGBB can be inferred, and the damage mechanism of the CGBB can be inverted. Therefore, the change of AE signal and resistivity may be used to monitor the stability of the CGBB in the goaf. However, most studies only qualitatively analyzed the AE signal and resistivity changes during the mechanical destruction of the CGBB. How to establish the quantitative relationship between the AE parameters, the resistivity, and the damage evolution process of the CGBB needs further research.

This research conducted uniaxial compression experimental tests on the strip and column CGBBs and analyzed the stress-strain relationship and failure characteristics. The AE technology was used to monitor the damage evolution, and a resistivity monitoring method was proposed for the special loading form of the CGBB. In addition, the discrete element simulation (Particle Flow Code) was used to analyze the damage and failure process of the strip CGBB and the influence of the length-height ratio on its strength and failure characteristics. According to the experimental results, the damage constitutive models of the strip and column CGBBs under uniaxial compression were established, and the stability monitoring models of the strip and column CGBBs were built based on

the resistivity and cumulative AE ring counts. This research can provide a certain reference for the design and stability monitoring of the CGBB in constructional backfill mining.

2. Experimental Specimen And Method

2.1 Specimen preparation

The cemented gangue backfill body (CGBB) was made of coal gangue aggregate (950 Kg/m³), 42.5 Ordinary Portland cement (190 Kg/m³), second class fly ash (380 Kg/m³), and tap water (350 Kg /m³) (Guo et al. 2020). Fly ash was taken from the thermal power plant of Fenxi Mining Group, China. Coal gangue was collected from Shanxi Tunlan Coal Mine, China. After secondary crushing, according to the nominal diameter, the coal gangue was divided into 3 groups (0 ~ 5 mm, 5 ~ 10 mm, 10 ~ 15 mm), which respectively account for 30%, 35%, and 35% of the total mass of the used coal gangue, as shown in Fig. 2. The fineness modulus of fine coal gangue aggregate (0 ~ 5 mm) was 3.10. The physical properties and chemical composition of fly ash and cement, and the particle size gradation of fly ash and coal gangue have been introduced in the literature (Ran et al. 2021). Using molds with dimensions of 300×100×100 mm and 150×150×150 mm, the strip and column CGBB specimens were cast, respectively. During the casting process, the conductive mesh with a size of 100×120 mm and 100×170 mm was placed in the strip and column molds in advance, respectively, as shown in Fig. 2. The conductive mesh has been introduced in the literature (Ran et al. 2021). The conductive mesh was used to monitor the internal damage evolution of the strip and column CGBBs during the uniaxial compression process (Guo et al. 2020). After casting for 24h, all samples were put in the standard curing room for 14d (Du et al. 2019b).

2.2 Testing method

A hydraulic servo-controlled test system (model: TAJW-2000) was used for the uniaxial compression test, the displacement loading method was adopted, and the loading rate was 0.8 mm/min, as shown in Fig. 2. An AE system (model: DS5-8B) was used to monitor the internal damage of the CGBB sample during the uniaxial compression process, and three probes were placed on the surface of the CGBB sample. Vaseline was used as the coupling agent between the probes and the testing CGBB sample. In addition, two types of conductive mesh arrangements were designed, as shown in Fig. 2. During uniaxial compression, the horizontally and the axially symmetrical arrangement conductive meshes tested the horizontal resistance and the axial resistance of the CGBB sample, respectively. The resistance between the two conductive meshes was recorded by a resistance measuring instrument (model: HPS2518A). This device can record the axial and horizontal resistance of the CGBB sample under the uniaxial compression process at an interval of 0.1 ms, thereby avoiding the mutual influence of the axial and horizontal current. The tested resistance and the electrical resistivity ρ obey the following equation:

$$\rho = RS/L$$

1

Where, S is the cross-sectional area of the test sample, and L is the distance between two pre-embedded conductive meshes in the CGBB sample (Liu et al. 2019). For the 150×150×150 mm specimen, $S = 0.015 \text{ m}^2$ and $L = 0.11 \text{ m}$; for the 100×100×300 mm specimen, $S = 0.01 \text{ m}^2$ and $L = 0.20 \text{ m}$.

3. Experimental Results And Discussion

3.1 Stress-strain curve and failure characteristics

3.1.1 Stress-strain curve

Figure 3 shows the stress-strain curves of strip and column CGBBs during the uniaxial compression process. There is a significant difference between the stress-strain curves of the strip and column CGBBs. The compaction stage of the column CGBB is significantly shorter than that of the strip CGBB, and the column CGBB quickly enters the elastic stage and reaches the peak stress. In the post-peak stage, the stress of the column CGBB decreases faster than that of the strip CGBB with the increase of strain. The peak stress and the corresponding peak strain of the strip CGBB are higher than those of the column CGBB. The average peak stress of the strip and column CGBBs is 5.73 MPa and 5.02 MPa, and the average peak strain of strip and column CGBBs is 0.0253 and 0.0094, respectively. The peak stress and peak strain of the strip CGBB are 1.14 and 2.69 times those of the column CGBB, respectively. The elastic modulus of the strip and column CGBBs were calculated based on the stress-strain relationship at the elastic stage. The average value of the elastic modulus of the strip CGBB was 0.43 times that of the column CGBB, by 438.77 MPa and 1020.14 MPa, respectively.

Obviously, the bearing capacity of the strip CGBB is higher than that of the column CGBB, and the ductility characteristics of the strip CGBB are better than that of column CGBB. Under the same stress conditions, the strip CGBB can produce greater axial deformation than the column CGBB, especially in the compaction stage, with the increase of strain, the stress of the strip CGBB increases slowly, and the adjustment of the stress field of the overlying strata is used to avoid local damage due to stress concentration, which gives full play to the bearing capacity of the overlying strata. In the post-peak stage, with the increase of strain, the decreasing rate of the stress of the strip CGBB is significantly lower than that of the column CGBB. The failure process of the strip CGBB has obvious characteristics of flexibility and can still bear relatively large stress under large deformations conditions, which avoids the overall sudden instability of the goaf due to the loss of the bearing capacity of the partial CGBBs and assures the overall stability of the goaf. This means that the short strip CGBB is more reliable than the column CGBB under the axial compression for keeping the stability of the goaf and should be more considered in the design of constructional backfill mining.

3.1.2 Failure properties

The failure characteristics of the column and strip CGBBs are shown in Fig. 4. The crack evolution process of the column CGBB under uniaxial compression is shown in Fig. 4a-c. The main cracks first appeared on the left and right sides of the CGBB specimen (regions I and II), and during the same period, more micro-

cracks were produced and developed. Main cracks and micro-cracks grew faster with the increase of strain, and then the middle position of the CGBB sample (region Ⅱ) continues to be squeezed and expanded, and cracks were generated. During the destruction process of the column CGBB sample, the four edges of the free surface firstly peeled off, and then the middle position of the sample was squeezed and expanded, and gradually peeled off. Finally, a core bearing area formed as shown in Fig. 4d. In the process of uniaxial compression, the column CGBB shortens vertically and expands horizontally. Because the elastic modulus and lateral deformation coefficients of the press plate and the CGBB sample surfaces are different, friction will be generated between the press plate and the end surfaces of the CGBB sample, which restricts the horizontal deformation of the ends of the CGBB sample, forming a hoop effect. This is consistent with the actual engineering conditions, due to the large friction coefficient of the rough roof and floor of the goaf, two opposite hyperbolic failure surfaces formed when the column CGBB is destroyed (Fig. 4d). However, there is little lateral constrain in the middle of the column CGBB, and therefore, arranging hoop stirrups in the middle of the column CGBB can enhance its bearing capacity (Du et al. 2019).

The failure properties of the strip CGBB are also affected by the hoop effect, as shown in Fig. 4e and f. During the uniaxial compression process, the CGBB specimen was continuously compressed in the Z direction, and continuously squeezed and expanded in the X and Y directions, but in the Y direction, due to the hoop effect and Poisson effect, the middle of the specimen was more constrained than that of the X direction. After the peak stress, the strip CGBB was squeezed and expanded continuously in the middle position, resulting in cracks, as shown in area III, and the surface of the CGBB continuously peeled off. At the I and II area of the strip CGBB, the same damage shape as the column CGBB specimen formed, similar to the hyperbolic type, and the outermost surface of the CGBB sample will continuously peel off. The strip CGBB peeled off from both sides inward layer by layer during the failure process and was severely damaged by extrusion on the free surface, as shown in Fig. 4g. Both sides (Y direction) have the effect of lateral pressure limiting due to the hoop effect, and the strip CGBB will mainly continue to expand in the X direction, so the squeeze expansion effect (X direction) of the strip CGBB is more obvious than that of the column CGBB. When the strip CGBB loses its bearing capacity, the surface of the strip CGBB will all peel off, forming the final core bearing area, as shown in Fig. 4h.

Figure 4i and j illustrate the failure mechanism of strip and column CGBBs under uniaxial compression. Because of the end restraint effect and Poisson effect, the center of the CGBBs will be squeezed by the confining pressure on the left and right sides. The confining pressure will decrease with the increase of the distance away from the middle, and it will form a one-way squeeze when it reaches the two ends; therefore, the CGBBs will be destroyed from the ends and destroyed layer by layer from both ends to the center. There are three reasons for the bearing capacity of the strip CGBB is better than that of the column CGBB. Firstly, compared with the column, the strip CGBB has better coordination and deformation ability, and will not cause catastrophic instability to the strip CGBB due to local damage. Secondly, after the outer layer of the strip CGBB is damaged, compared with the column CGBB, the strip CGBB has a larger core bearing area. Herein, the real internal stress of the strip CGBB under pressure increases at a lower speed and the damage rate of the core bearing area is also less than that of a single column CGBB. Finally, after the outer layer of strip CGBB is partially damaged, the core bearing area will still have a certain bearing capacity due to the side pressure limit of the outermost CGBB part. Overall, the short strip CGBB should be considered firstly in the design of constructional backfill mining to improve the overall stability of the CGBB system.

3.2 Acoustic emission characteristics

Once the stress-strain curve enters the post-peak stress stage, under the constant load of the roof, the CGBB is quickly destroyed, and there will not show the post-peak stress-strain curve by displacement loading using a hydraulic servo-controlled test system. Therefore, to monitor the stability of the CGBB by using the AE signal before the peak stress in constructional backfill mining, this research does not analyze the AE characteristics of the CGBB at the post-peak stress stage.

3.2.1 Strip cemented gangue backfill body

The change of the AE ring counts, energy, accumulated ring counts, and accumulated energy over time in the uniaxial compression process of the strip CGBB is shown in Fig. 5. In Fig. 5a, it is clear that the AE ring counts and energy present an increase-decrease-increase trend before the peak stress. In the initial loading stage, the internal pores of the strip CGBB are gradually compacted, large gaps or even crushed, and meantime, there is friction between the aggregate and the cement matrix, so that small energy events can be stably generated during the compaction stage, and accompanied the occurrence of microcracks. After the strip CGBB is compacted, it gradually enters the elastic phase. The strain energy stored in CGBB gradually grows until the strain energy exceeds the energy required for crack propagation. Subsequently, with the continuous accumulation of strain energy and the expansion of microcracks, the strip CGBB enters the plastic stage and gradually reaches the peak stress. At the peak stress, because the core bearing area is restricted by the lateral pressure, and can not be destroyed suddenly; therefore, the AE ring counts and energy will not change drastically.

Figure 5b shows that the accumulative AE ring counts and accumulative energy gradually increase with the increase of stress, but the growth rate gradually decreases until it tends to be constant. The accumulative ring counts and accumulative energy curve of the strip CGBB did not show a sharp increase near the peak stress. The main reason is that the existence of the confining pressure suppressed the instantaneous release of the strain energy accumulated in the earlier stage of the strip CGBB, and the strip CGBB also will not lose stability instantaneously, which means that the strip CGBB has enough bearing capacity after the peak stress.

3.2.2 Column cemented gangue backfill body

The evolution of AE ring counts, energy, cumulative ring counts, and cumulative energy changes over time during the uniaxial compression of the column CGBB is shown in Fig. 6. It can be seen from Fig. 6a that, compared with Fig. 5a, the AE ring counts and energy have no obvious rising stage in the initial loading process. It is consistent with the features shown in the stress-strain curve, i.e., the initial compaction stage of the column CGBB is much shorter than that of the strip column, and thus there is no obvious rising period. AE ring counts and energy present a decline-crack adjustment-active stage until the column CGBB enters the post-peak stress stage. In the initial compaction stage, similar to the strip CGBB, the column CGBB can quickly generate small energy events, and then the column CGBB enters the elastic phase, and the number of AE events gradually decreases. Compared with the strip CGBB, in the compaction

stage, the AE ring counts and energy of the strip CGBB are larger than those of the column CGBB and more active. In the crack adjustment stage, the column CGBB continuously accumulates strain energy. Because there is little confining pressure effect, some cracks inside the column CGBB extend suddenly due to stress concentration, causing AE ring counts and energy increase. However, when this part of the strain energy is released, the column CGBB will calm down again. As the strain energy continues to accumulate, it gradually enters the active stage. When the accumulated strain energy exceeds the maximum energy that the column CGBB can bear, compared with the strip CGBB, the column CGBB destructs suddenly. Because there is little lateral confinement, the accumulated strain energy will be released instantaneously, so AE ring counts and energy will suddenly increase near the peak stress. In actual engineering, when the column CGBB enters the post-peak stage, the roof will continuously move down until the column CGBB is destroyed because there is little lateral restraint, which may cause the sudden instability of the goaf.

It can be seen from Fig. 6b that the evolution process of the cumulative AE ring counts and cumulative energy of the column CGBB are basically the same as the strip CGBB with time. However, when near the peak stress, because the column CGBB has little confining pressure, it is destroyed quickly and the energy is released instantly, a large number of cracks extend and penetrate, and finally, the cumulative AE ring counts and energy will increase suddenly.

3.3 Resistivity characteristics

3.3.1 Strip cemented gangue backfill body

The change of the horizontal resistivity of the strip CGBB during the uniaxial compression is shown in Fig. 7. It is obvious that the resistivity increases gradually with the increase of the stress before the peak stress. The resistivity changes little in the compaction and elastic stages, and increases in a small amount. However, after entering the plastic stage, the resistivity increases rapidly. The resistivity is sensitive at the peak of the stress-strain curve. When the stress reaches the peak stress, the resistivity also increases rapidly to the peak, and then after the peak stress, the resistivity has a rapid downward trend. This means that macroscopic cracks formed inside the strip CGBB along the axial direction, and the stress inside the strip CGBB is released. Next, the original large number of micro-cracks close instantaneously in the strip CGBB, and finally, the conductive path will increase. In addition, this demonstrates that the strip CGBB does not have many macrocracks at the peak stress, and it still has enough bearing capacity. After the peak stress, more macrocracks are continuously generated in the strip CGBB with the increase of axial strain, and the resistivity will increase again. The evolution of horizontal resistivity during the uniaxial compression process is consistent with the damage process of the strip CGBB, especially before the peak stress, which could be used to monitor the stability of the CGBB.

3.3.2 Column cemented gangue backfill body

The change of the axial and horizontal resistivity of the column CGBB with time in the uniaxial compression process is shown in Fig. 8a. The horizontal resistivity increases gradually with the increase of stress in the compacting and elastic stages. Furthermore, the horizontal resistivity is more sensitive in the plastic stage, and the growth rate increases gradually. When the peak stress is reached, the resistivity also increases sharply. After the peak stress, the evolution process of the horizontal resistivity of the column CGBB is similar to that of the strip CGBB, and all have a rapid decline trend. This is a typical feature point for the stability monitoring of the strip and column CGBBs, which can be used to judge whether the stress reaches its peak. The axial resistivity shows a similar changing process with the horizontal resistivity (Li et al. 2014; Hu et al. 2021), but the change range is much smaller and not obvious.

Compared to the horizontal resistivity with axial resistivity, it is obvious that the change of horizontal electrical resistivity tested by the horizontally symmetrically arranged conductive mesh is more sensitive to the damage inside the CGBB than that of the axially arranged conductive mesh. The cracks generated inside the CGBB can be sensed by the horizontal resistivity more quickly and accurately. This phenomenon is related to the producing mechanism of internal cracks in the CGBB, as shown in Fig. 8b. During uniaxial compression, the crack direction tends to be parallel to the loading direction of pressure. Therefore, the effective conductive area along the axial section becomes smaller, the conductive path decreases, and the horizontal resistivity continues to increase. Consequently, the horizontal resistivity can be more sensitive to perceive the damage evolution process inside the CGBB. This stability monitoring method with horizontally symmetrically arranged conductive mesh could be used in actual engineering because of the low cost and high sensitivity.

4. Numerical Simulation Analysis

Due to the constraints of the test conditions, it is difficult to study the damage and failure process of the strip CGBB with a large length-height ratio under the axial compression through the experiment. Therefore, the discrete element simulation (PFC software) was used to analyze the mechanical properties of the strip CGBB (with a length-height ratio of 1 ~ 9) under uniaxial compression. The influence of the length-height ratio on the failure characteristics of CGBB was studied, and the relationship between the length-height ratio and the strength of the CGBB was determined.

CGBBs are viscoelastic plastic bodies, and the linear parallel bond model can well reflect the elastoplasticity of the cemented materials (Li et al. 2021). Therefore, the lineal parallel bond model was adopted in this simulation. After the initial test model servo is completed, according to the elastic modulus obtained from the actual stress-strain curve and the strength of the strip and column CGBBs, the microscopic parameters of the numerical model were calibrated (Potyondya et al. 2004). Table 1 shows the mesoscopic parameters of the numerical model of CGBBs. The particle size is $0.5 \times 10^{-3} \sim 0.75 \times 10^{-3}$ m, and the porosity is 0.1. During the simulation process, the axial stress and strain of the strip CGBB and the change of the number of cracks were monitored, and the loading was stopped when the stress dropped to 70% of the peak stress.

Table 1
Model of microscopic parameters.

Shape	Basic property		Linear group			Parallel-bond group				Dashpot group	
	Density kg/m ³	Damp	Effective modulus E^* (GPa)	Normal-to-shear stiffness ratio k^*	Friction coefficient μ	Bonding effective modulus(GPa) E^*	Bond normal-to-shear stiffness ratio k^*	Bond tensile stress(MPa) σ_c	Bond cohesion(MPa) c	Friction angle ϕ	Normal critical damping ratio β_n
Column	2500	0.7	0.5	1.4	0.577	0.5	1.4	1.3	2.8	0	0.5
Strip	2500	0.7	0.22	1.5	0.577	0.22	1.5	1.6	3.0	0.2	0.5

4.1 Crack evolution process and influence of length-height ratio on failure characteristics

Take the overall failure process of the strip CGBB with a length-height ratio of 9 and the evolution process of the core bearing area as an example for illustration, as shown in Fig. 9a. Before the peak stress, during the initial loading process, the entire strip CGBB bears the load; with the continuous increase of the stress, the two ends of the strip CGBB are destroyed firstly, and the two ends gradually fall off. After the peak stress, due to the horizontal extrusion of the two ends, the core bearing area is formed, and then the core bearing area gradually decreases with increasing strain. The failure feature of the numerical simulation is consistent with the experimental results. Furthermore, the destruction process of the strip CGBB before the peak stress is consistent with the resistivity monitoring results. The horizontal resistivity of the strip CGBB increased rapidly in the plastic phase and reaches the maximum value at the peak stress, which means that the cracks increase with the increase of stress and macrocracks form at the peak stress.

The failure characteristics of strip CGBB specimens with different length-height ratios and the core bearing area are shown in Fig. 9b. The strip CGBBs with different length-height ratios show the same failure patterns, and the ends of the CGBB destroy firstly, and then multiple oblique shear monomers will gradually form at both ends of the strip CGBB. The number of cracks at both ends is more than that of the core bearing area. The core bearing area is subjected to the pressure limiting effect at both ends, and thus the core bearing area continues to bear the load under mutual squeezing and occlusion. Therefore, the strip CGBB still has a better bearing capacity in the post-peak stage than the column CGBB, showing obvious ductility characteristics.

4.2 Influence of length-height ratio on the strength

The stress-strain curve of strip CGBB with different length-height ratios is shown in Fig. 10a. Both the strength and peak strain of the strip CGBB increase gradually with the increase of length-height ratio. Besides, as the length-height ratio increases, the ductility of the strip CGBB gradually increases, and the stress at the post-peak decreases more slowly, and even the characteristic of strain hardening appears gradually.

The change process of the number of cracks per unit volume with strain is shown in Fig. 10b. Few cracks occurred in the early stage of loading. After entering the plastic stage, the number of cracks gradually increases with the increase of strain; and then entering the post-peak stage, it increases approximately linearly. In addition, the growth rate of the number of cracks of the column CGBB is higher than that of the strip CGBB, which reflects the quasi-brittle characteristic of the instability of the column CGBB. This is because the strip CGBB can be restrained by the lateral pressure due to the hoop effect and lateral Poisson effect. The growth rate of the number of cracks per unit volume is also related to the length-height ratio. The larger the length-height ratio is, the slower the growth rate will be. Due to the effect of confining pressure, the strip CGBB shows obvious ductility characteristics, avoiding sudden instability as the column CGBB.

According to the numerical simulation results, the relationship between the length-height ratio and uniaxial compressive strength of the strip CGBB is fitted, as shown in Fig. 11. The strength increases with the increase of length-width ratio, but the increasing ratio decreases gradually and the strength of the strip CGBB may reach a constant finally. This model could be used to calculate the strength of the strip CGBB under different length-height ratios.

5. Stress-strain Constitutive Model Of Cemented Gangue Backfill Body

Under the action of external pressure, the deterioration of materials or structures caused by the development of micro-defects at the mesostructure level is called damage. In the late 1970s, Lemaitre et al. proposed continuous damage mechanics based on the material damage process and established a damage model (Wang et al. 2020):

$$\sigma = E(1 - D)\varepsilon$$

where σ is the effective stress; D is the damage variable; E is the elastic modulus; ε is the strain.

Based on the Weibull statistical distribution function (Liu et al. 2018), the damage evolution equation of material can be written as:

$$D = 1 - \exp\left(-\frac{\varepsilon^m}{\alpha}\right) \quad (3)$$

Where m and α are constants associated with dimensions and scale of the sample, respectively.

Under the uniaxial compression, the constitutive model parameters are determined by the following method (Deng et al. 2006):

$$m = 1 / \ln \left(\frac{E \varepsilon_p}{\sigma_p} \right), \quad \alpha = m \varepsilon_p^m$$

4
Where σ_p is the peak stress, MPa; ε_p is the peak strain; E is the elastic module, MPa.

Therefore, the damage variable can be defined as:

$$D = 1 - \exp \left[- \frac{1}{m} \left(\frac{\varepsilon}{\varepsilon_p} \right)^m \right] \quad (5)$$

Based on the above, the damage constitutive model of CGBB under uniaxial compression can be expressed as:

$$\sigma = E \varepsilon \left\{ \exp \left[- \frac{1}{m} \left(\frac{\varepsilon}{\varepsilon_p} \right)^m \right] \right\} \quad (6)$$

According to the stress-strain curves of strip and column CGBBs obtained in the experiment, the elastic modulus, peak strain, peak stress, etc., are calculated, as shown in Table 2. Substituting the parameters in Table 2 into equation (6), the damage constitutive equations of strip and column CGBBs under uniaxial compression can be obtained. The model and experimental stress-strain curve and the change process of damage factor with strain are shown in Fig. 12. It can be seen that, in general, this model could depict the stress-strain curve and damage model both of the strip and column CGBBs.

Table 2
Measured parameters and equation of damage constitutive models under uniaxial compression.

Sample	σ_p	ε_p	E	m	Damage constitutive model
Strip	5.716	0.0235	369.7	2.398	$\sigma = 369.7 \varepsilon \exp \left[- \frac{1}{2.398} \left(\frac{\varepsilon}{0.0235} \right)^{2.398} \right]$
Column	5.281	0.00963	959.1	1.789	$\sigma = 956.1 \varepsilon \exp \left[- \frac{1}{1.789} \left(\frac{\varepsilon}{0.00963} \right)^{1.789} \right]$

6. Stability Monitoring Model Of Cemented Gangue Backfill Body

According to the analysis in Section 3.2, the change of the AE ring counts can characterize the entire process of instability and destruction of the strip and column CGBBs. In addition, according to the analysis in Section 3.3, before the peak stress, with the increase of the stress, the resistivity also increases gradually. When the peak stress is reached, the resistivity of the CGBB suddenly increases to the maximum value. The above features can be regarded as the characteristic points of the instability of the CGBB to realize the stability monitoring of the strip and column CGBBs in constructional backfill mining. In the process of monitoring the stability of the CGBB, the accumulative AE ring counts and resistivity could be used to judge the stress, strain, and damage state of the CGBB, to realize the stability monitoring of the strip and column CGBBs in the goaf. Therefore, it is necessary to establish the relationship between cumulative ring counts, resistivity and stress, strain, and damage.

The damage constitutive model of the rock based on the cumulative AE ring counts can be established (Wu et al. 2015). This uniaxial compression test adopts the displacement loading method, and the relationship between strain and time is linear. Therefore, the relationship between strain ε and time t is:

$$\varepsilon = kt + \varepsilon_0$$

7
Where k is the strain rate; ε_0 is the initial strain.

As shown in Fig. 5(b) and Fig. 6(b), the relationship between cumulative AE ring counts N and time t can be expressed by the index function:

$$N = A_1 \exp \left(- \frac{t}{B} \right) + A_2$$

8
Where A_1 , A_2 , and B are determined by the fitting results of experimental results.

The relationship between cumulative AE ring counts N and strain ε can be obtained by combining the formula (7) and (8).

$$\varepsilon = \varepsilon_0 - B \ln \left(\frac{N - A_2}{A_1} \right)$$

9
Therefore, according to formula (3) and formula (9), the damage variable can be defined as:

$$D = 1 - \exp \left\{ -\frac{1}{\alpha} \left[\varepsilon_0 - B \ln \left(\frac{N - A_2}{A_1} \right) \right]^m \right\}$$

10
According to formula (2) and formula (10), the relationship between cumulative AE ring counts and stress σ of the CGBB is:

$$\sigma = E \left[\varepsilon_0 - B \ln \left(\frac{N - A_2}{A_1} \right) \right] \exp \left\{ -\frac{1}{\alpha} \left[\varepsilon_0 - B \ln \left(\frac{N - A_2}{A_1} \right) \right]^m \right\}$$

11
The model parameters were fitted by the column CGBB, and the fitting results are shown in Table 3. The relationship between the stress, strain, and damage factors of the theory is plotted in Fig. 13a.

Similarly, as shown in Fig. 7, the relationship of the resistivity ρ and time can be expressed as:

$$\rho = D_1 \exp \left(-\frac{t}{H_1} \right) + F$$

12
Where $D_1, H_1,$ are determined by the fitting results of experimental data.

Combination of the formula (7) and formula (12), the relationship between resistivity ρ and strain ε is:

$$\varepsilon = \varepsilon_0 - H_1 \ln \left(\frac{\rho - F}{D_1} \right)$$

13
Combination of the formula (13) and formula (3), the relationship between damage variable and resistivity and the relationship between stress and resistivity are:

$$D = 1 - \exp \left\{ -\frac{1}{\alpha} \left[\varepsilon_0 - H_1 \ln \left(\frac{\rho - F}{D_1} \right) \right]^m \right\}$$

14
Combination of the formula (14) and formula (2), the relationship between stress σ and resistivity ρ can be expressed as:

$$\sigma = E \left[\varepsilon_0 - H_1 \ln \left(\frac{\rho - F}{D_1} \right) \right] \exp \left\{ -\frac{1}{\alpha} \left[\varepsilon_0 - H_1 \ln \left(\frac{\rho - F}{D_1} \right) \right]^m \right\}$$

15
The horizontal resistivity monitoring result of the strip CGBB specimen was selected to verify the stability monitoring model of resistivity. Table 3 shows the calculation parameters. This model calculation results and experimental data are shown in Fig. 13b.

It can be seen from Fig. 13 that the experimental data and the model calculation results are in good agreement as a whole, while the consistency is not very high in the compaction stage of the strip and column CGBBs. Therefore, these models can be used in the stability monitoring of CGBB in constructional backfill mining.

Table 3
The parameters of acoustic emission cumulative ring counts model and resistivity model.

Acoustic emission cumulative ring	σ_p /MPa	ε_p	/MPa	α		ε_0	A_1	A_2		
Parameter value	5.1223	0.00992	1137.8	3.686E-3	1.265	8.886E-5	1.869E-4	-4102.72	39.66	3996.32
Resistivity	σ_p /MPa	ε_p	/MPa	α		ε_0	D_1	H_1		
Parameter value	5.854	0.0298	373.7	6.594E-3	1.555	1.3324E-4	0.0024	11.392	-34.58	26.193

7. Conclusions

(1) The strength and peak strain of strip CGBB is 1.14 times and 2.69 times those of column CGBB, respectively. The strip CGBB shows stronger ductility than the column CGBB. Both strip and column CGBBs have a core bearing area under uniaxial compression. The decline rate of the stress of column CGBB after the peak stress is significantly greater than that of strip CGBB. At the post-peak stage, the strip CGBB can still bear a large load under the large deformation. During the failure process, the strip CGBB peels off from both sides inward layer by layer and is severely damaged by extrusion on the free surface, and the column CGBB will form an opposite hyperbolic failure surface.

(2) The strength and ductility of the strip CGBB increase with the increase of the length-height ratio, and the relationship between length-height ratio and strength is established. The growth rate of the crack number per unit volume of the column CGBB is higher than that of the strip CGBB, and the larger the length-height ratio of the strip CGBB is, the slower the crack growth rate will be. With the increase of axial strain, both ends of the strip CGBB are damaged firstly, and gradually expand to the center, the core bearing area decreases correspondently, and finally, multiple oblique shear parts will gradually form at both ends.

(3) The AE evolution process of strip and column CGBBs under uniaxial compression before the peak stress can be divided into three stages, respectively. Compared with column CGBB, the AE ring counts and energy of strip CGBB at the peak stress will not increase sharply. The resistivity monitoring effect of the conductive mesh arranged horizontally symmetrically is better than that of the axial. The horizontal resistivity increases slowly in the compaction and elastic stages, and increases rapidly in the plastic stage and increases suddenly at the peak stress, and then drops rapidly after the peak stress.

(4) According to the stress-strain curves of the strip and column CGBBs under uniaxial compression, the damage constitutive models of the strip and column CGBBs are established. Meantime, the stability monitoring models of the CGBBs under uniaxial compression are established based on the cumulative AE ring counts and resistivity, respectively.

Declarations

Availability of data and materials

The datasets used and/or analyzed during the current study are available from the corresponding author on reasonable request.

Author contribution

Hongyu Ran: conceptualization, Experiment, investigation, and writing-original draft. Yuxia Guo: funding acquisition, methodology, and writing review and editing. Guorui Feng: investigation, supervision, funding acquisition. Chunqing Li: writing-review and editing.

Funding

This work is supported by the National Natural Science Foundation of China (51974192), Distinguished Youth Funds of National Natural Science Foundation of China (51925402), Shanxi Science and Technology Major Project (20201102004). Thanks for all the support for this basic research.

Ethics approval Not applicable

Consent to participate Not applicable

Consent for publication Not applicable

Competing interest The authors declare no competing interests

References

1. Chen SJ, Yin DW, Cao FW, Liu Y, Ren KQ (2016) An overview of integrated surface subsidence-reducing technology in mining areas of China. *Nat Hazards* 81(2):1129–1145. <https://doi.org/10.1007/s11069-015-2123-x>
2. Chen SJ, Yin DW, Hu BN, Yang HS, Yin XW (2020) Study on mechanical characteristics of composite system of hard roof and filling body under strip filling. *Journal of Mining & Safety Engineering* 37(01):110–117. (In Chinese) <https://doi.org/10.13545/j.cnki.jmse.2020.01.012>
3. Du XJ, Feng GR, Zhang YJ, Wang ZH, Guo YX, Qi TY (2019a) Bearing mechanism and stability monitoring of cemented gangue-fly ash backfill column with stirrups in partial backfill engineering. *Engineering Structure* 188:603–612. <https://doi.org/10.1016/j.engstruct.2019.03.061>
4. Du XJ, Feng GR, Qi TY, Guo YX, Zhang YJ, Wang ZH (2019b) Failure characteristics of large unconfined cemented gangue backfill structure in partial backfill mining. *Constr Build Mater* 194:257–265. <https://doi.org/10.1016/j.conbuildmat.2018.11.038>
5. Du XJ, Feng GR, Qi TY, Guo YX, Wang ZH, Zhang YJ, Li Zhen, Bai JW (2019c) Roof stability analyses of “water-preserved and water-stored” coal mining with constructional backfill mining. *Journal of China Coal Society* 44(003):820–829. (In Chinese) <https://doi.org/10.13225/j.cnki.jccs.2018.6024>
6. Deng DQ, Yang YL, Yao ZL (2006) Research on constitutive equation of damage evolution of backfill based on the full tensile and compressive process. *Journal of Mining & Safety Engineering*(04):485–488. (In Chinese)
7. Feng GR, Du XJ, Guo YX, Qi TY, Wang ZH, Li QD, Li HY, Kang LX (2019) Basic theory of constructional backfill mining and the underground space utilization concept. *Journal of China Coal Society* 44(01):74–84. (In Chinese) <https://doi.org/10.13225/j.cnki.jccs.2018.1598>

8. Feng GR, Zhang YJ, Qi TY, Kang LX (2020) Status and research progress for residual coal mining in China. *Journal of China Coal Society* 45(01):151–159. (In Chinese) <https://doi.org/10.13225/j.cnki.jccs.YG19.1280>
9. Guo YX, Ran HY, Feng GR, Du XJ, Qi TY, Wang ZH (2020) Effects of curing under step-by-step load on mechanical and deformation properties of cemented gangue backfill column. *Journal of Central South University* 27(11):3417–3435. <https://doi.org/10.1007/s11771-020-4556-y>
10. Guo YX, Ran HY, Feng GR, Du XJ, Zhao YH, Xie WS (2021a) Deformation and instability properties of cemented gangue backfill column under step-by-step load in constructional backfill mining. *Environmental Science and Pollution Research* (2021). <https://doi.org/10.1007/s11356-021-15638-z>
11. Guo YX, Zhao YH, Wang SW, Feng GR, Zhang YJ, Ran HY (2021b) Stress-strain-acoustic responses in failure process of coal rock with different height to diameter ratios under uniaxial compression. *Journal of Central South University* 28(6):1724–1736. <https://doi.org/10.1007/s11771-021-4729-3>
12. Hu QT, Song MY, Li QG, Wu YQ, Xu YC, Zhang YB, Deng YZ (2021) Analysis of resistivity response of stratified briquette during uniaxial compression. *Journal of China Coal Society* 46(01):211–219. (In Chinese) <https://doi.org/10.13225/j.cnki.jccs.2020.1870>
13. Hou JF, Guo ZP, Li JB, Zhao LJ (2020) Study on triaxial creep test and theoretical model of cemented gangue-fly ash backfill under seepage-stress coupling. *Constr Build Mater* 273:121722. <https://doi.org/10.1016/j.conbuildmat.2020.121722>
14. Li SC, Xu XJ, Liu ZY, Yang WM, Liu B, Zhang X, Wang ZC, Nie LC, Li JL, Xu L (2014) Electrical resistivity and acoustic emission response characteristics and damage evolution of sandstone during whole process of uniaxial compression. *Chin J Rock Mech Eng* 33(01):14–23. (In Chinese) <https://doi.org/10.13722/j.cnki.jrme.2014.01.002>
15. Li Y, Qiang S, Xu WQ, Hua X, Xu C, Lai JY, Yuan M, Chen B (2021) Verification of concrete nonlinear creep mechanism based on meso-damage mechanics. *Constr Build Mater* 276:122205. <https://doi.org/10.1016/j.conbuildmat.2020.122205>
16. Liu XS, Tan YL, Ning JG, Lu YW, Gu QH (2018) Mechanical properties and damage constitutive model of coal in coal-rock combined body. *Int J Rock Mech Min Sci* 110:140–150. <https://doi.org/10.1016/j.ijrmms.2018.07.020>
17. Liu Q, Xu WX, Xiao JZ, Tian YT, Chen JY, Singh A (2019) Correlation between damage evolution and resistivity reaction of concrete in-filled with graphene nanoplatelets. *Constr Build Mater* 208:482–491. <https://doi.org/10.1016/j.conbuildmat.2019.03.036>
18. Liu JG, Li XW, He T (2020) Application status and prospect of backfill mining in Chinese coal mines. *Journal of China Coal Society* 45:141–150. (In Chinese) <https://doi.org/10.13225/j.cnki.jccs.YG19.1063>
19. Potyondya DO, Cundall PA (2004) A bonded-particle model for rock. *Int J Rock Mech Min Sci* 41:1329–1364. <https://doi.org/10.1016/j.ijrmms.2004.09.011>
20. Ran HY, Guo YX, Feng GR, Qi TY, Du XJ (2021) Creep properties and resistivity-ultrasonic-AE responses of cemented gangue backfill column under high-stress area. *International Journal of Mining Science and Technology*, 2021 31(3):401–412. <https://doi.org/10.1016/j.ijmst.2021.01.008>
21. Sun Q, Li B, Tian S, Cai C, Xia YJ (2018a) Creep properties of geopolymer cemented coal gangue-fly ash backfill under dynamic disturbance. *Constr Build Mater* 191:644–654. <https://doi.org/10.1016/j.conbuildmat.2018.10.055>
22. Sun Q, Zhang JX, Zhou N (2018b) Study and discussion of short-strip coal pillar recovery with cemented paste backfill [J]. *Int J Rock Mech Min Sci* 104:147–155. <https://doi.org/10.1016/j.ijrmms.2018.01.031>
23. Sun Q, Cai C, Zhang SK, Tian S, Li B, Xia YJ, Sun QW (2019) Study of localized deformation in geopolymer cemented coal gangue-fly ash backfill based on the digital speckle correlation method. *Constr Build Mater* 215:321–331. <https://doi.org/10.1016/j.conbuildmat.2019.04.208>
24. Wu XZ, Liu JW, Liu XX, Zhao K, Zhang YB (2015) Study on the coupled relationship between AE accumulative ring-down counts and damage constitutive model of rock. *Journal of Mining & Safety Engineering* 32(01):28–3441. (In Chinese) <https://doi.org/10.13545/j.cnki.jmse.2015.01.005>
25. Wu JY, Jing HW, Yin Q, Yu LY, Meng B, Li SC (2020) Strength prediction model considering material, ultrasonic and stress of cemented waste rock backfill for recycling gangue. *J Clean Prod* 276:123189. <https://doi.org/10.1016/j.jclepro.2020.123189>
26. Wu JY, Gao YQ, Meng Y, Jing B HW (2021a) Particle size distribution of aggregates effects on mesoscopic structural evolution of cemented waste rock backfill. *Environ Sci Pollut Res* 28:16589–16601. <https://doi.org/10.1007/s11356-020-11779-9>
27. Wu JY, Jing HW, Meng QB, Yin Q, Yu LY (2021b) Assessment of cemented waste rock backfill for recycling gangue and controlling strata: creep experiments and models. *Environ Sci Pollut Res* 28:35924–35940. <https://doi.org/10.1007/s11356-021-12944-4>
28. Wang F, Jiang BY, Chen SJ, Ren MZ (2018) Surface collapse control under thick unconsolidated layers by backfilling strip mining in coal mines. *Int J Rock Mech Min Sci* 113:268–277. <https://doi.org/10.1016/j.ijrmms.2018.11.006>
29. Wang J, Fu JX, Song WD, Zhang YF, Wang Y (2020) Mechanical behavior, acoustic emission properties and damage evolution of cemented paste backfill considering structural feature. *Constr Build Mater* 261:119958. <https://doi.org/10.1016/j.conbuildmat.2020.119958>
30. Xu JL, You Q, Zhu WB, Li XS, Lai WQ (2007) Theoretical study of strip-filling to control mining subsidence. *Journal of China Coal Society* 32(2):119–122. (In Chinese)
31. Xu JL, Xuan DY, Zhu WB, Wang XZ, Wang BL, Teng H (2015) Study and application of coal mining with partial backfilling. *Journal of China Coal Society* 40(06):1303–1312. (In Chinese) <https://doi.org/10.13225/j.cnki.jccs.2015.3055>
32. Xu WB, Hou YB, Song WD, Zhou YP, Yin TJ (2016) Resistivity and thermal infrared precursors associated with cemented backfill mass. *Journal of Central South University* 23(9):2329–2335. <https://doi.org/10.1007/s11771-016-3291-x>
33. Yang K, Zhao XY, Wei Z, Zhang JQ (2021) Development overview of paste backfill technology in China's coal mines: a review. *Environmental Science and Pollution Research* (2021). <https://doi.org/10.1007/s11356-021-16940-6>
34. Zhang QL, Wang XM (2007) Performance of cemented coal gangue backfill. *Journal of Central South University of Technology* 14(2):216–219. <https://doi.org/10.1007/s11771-007-0043-y>

35. Zhang XG, Lin J, Liu JX, Li F, Pang ZZ (2017) Investigation of Hydraulic-Mechanical Properties of Paste Backfill Containing Coal Gangu-Fly Ash and Its Application in an Underground Coal Mine. *Energies* 10(9):19. <https://doi.org/10.3390/en10091309>
36. Zhang JX, Zhang Q, Ju F, Zhou N, Li M, Zhang WQ (2019) Practice and technique of green mining with integration of mining, dressing, backfilling and X in coal resources. *Journal of China Coal Society* 44(01):64–73. (In Chinese) <https://doi.org/10.13225/j.cnki.jccs.2018.5045>
37. Zhu WB, Xu JM, Xu JL, Chen DY, Shi JX (2017) Pier-column backfill mining technology for controlling surface subsidence. *Int J Rock Mech Min Sci* 96:58–65. <https://doi.org/10.1016/j.ijrmms.2017.04.014>
38. Zhu XJ, Guo GL, Liu H, Yang XY (2019) Surface subsidence prediction method of backfill-strip mining in coal mining. *Bull Eng Geol Environ* 78:6235–6248. <https://doi.org/10.1007/s10064-019-01485-3>
39. Zhu XJ, Guo GL, Li H, Chen T, Yang XY (2020) Roof-breaking mechanism and stress-evolution characteristics in partial backfill mining of steeply inclined seams. *Geomatics Natural Hazards & Risk*. <https://doi.org/10.1080/19475705.2020.1823491>. 11:2006-2035

Figures

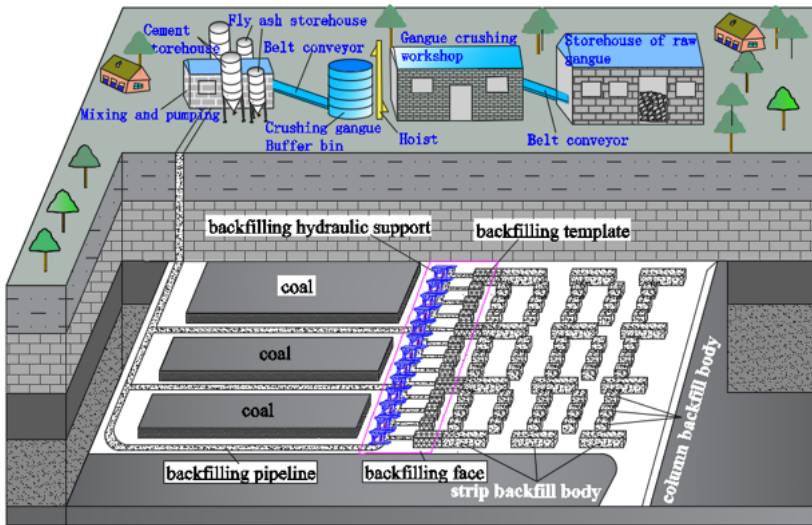


Figure 1

Diagram of constructional backfill mining of coal mining.

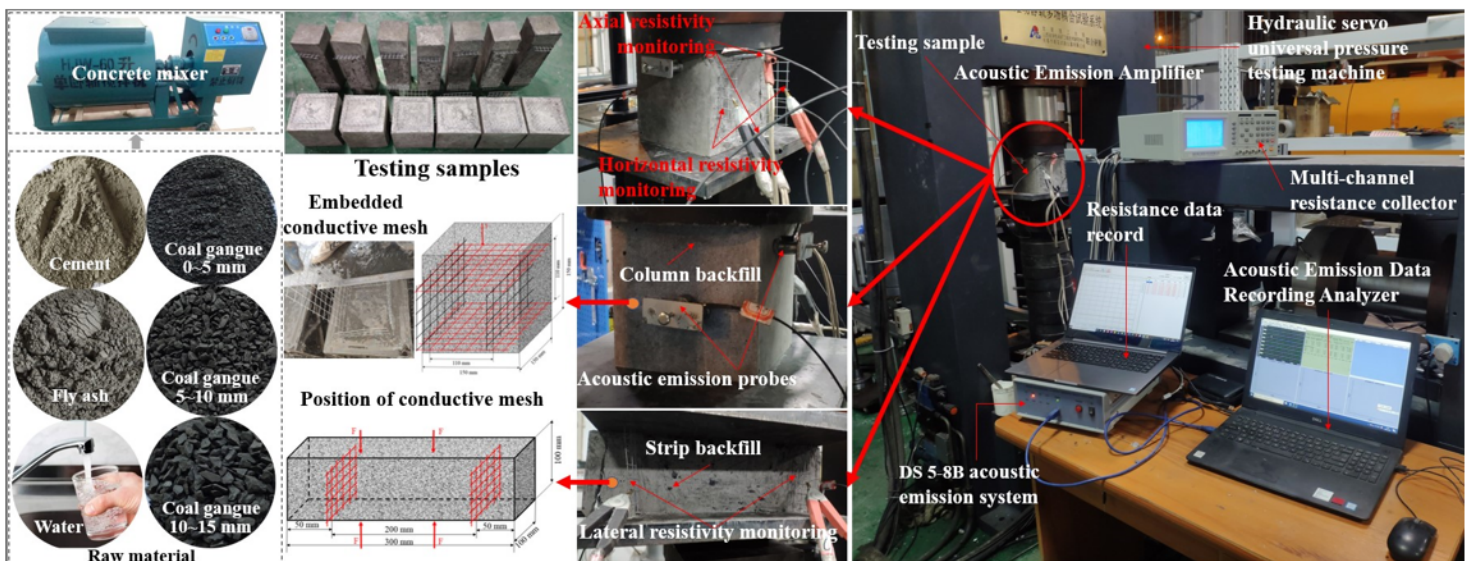


Figure 2

Experimental system for the preparation process of samples and the uniaxial compression tests.

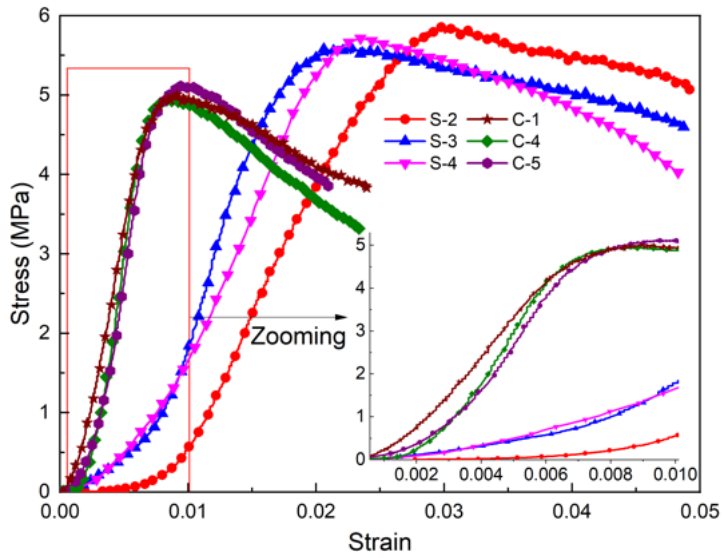


Figure 3
Stress-strain curves of strip and column cemented gangue backfill bodies.

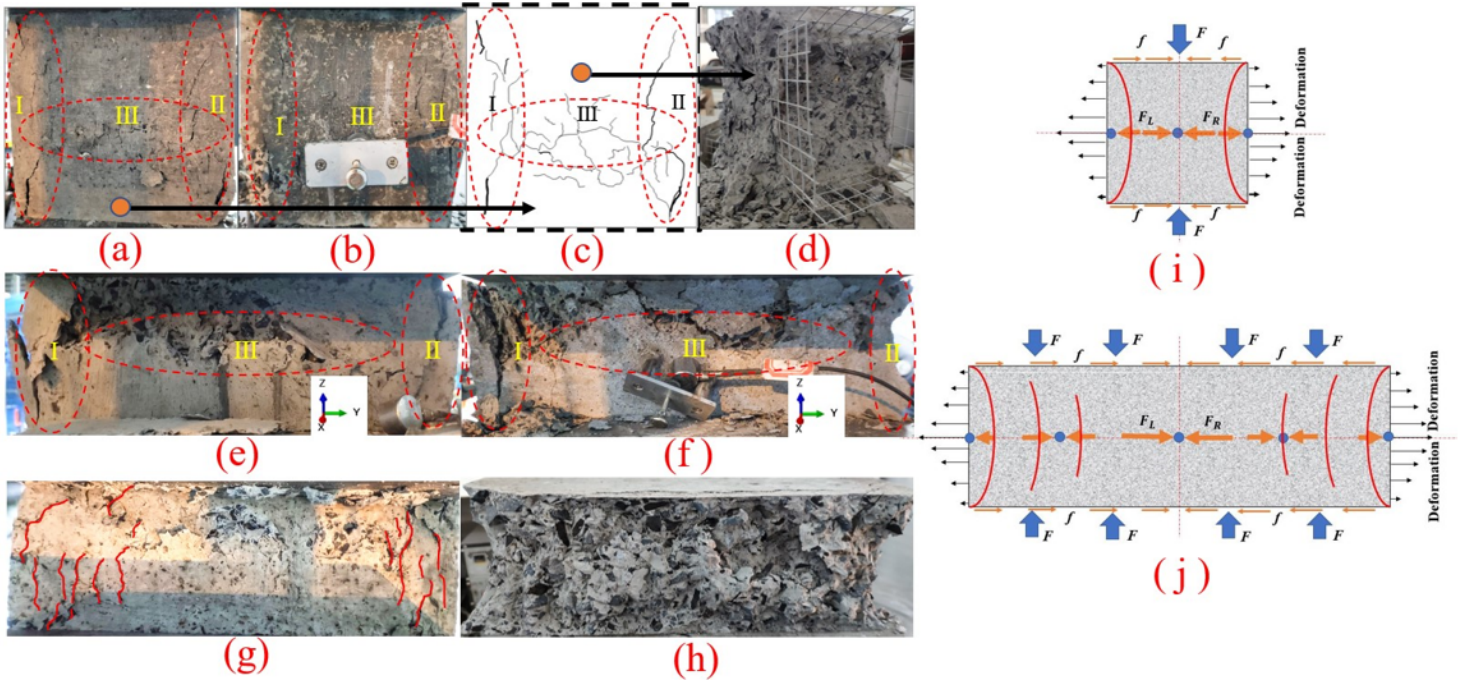


Figure 4
The failure characteristics of column and strip cemented gangue backfill bodies.

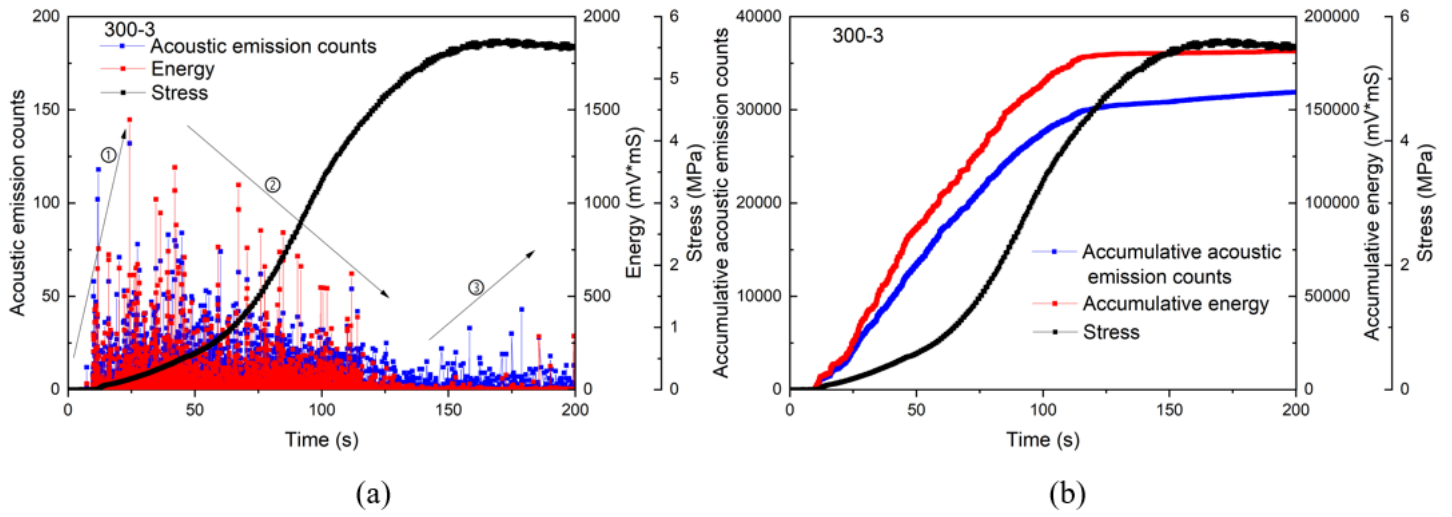


Figure 5

AE characteristics of strip cemented gangue backfill body under uniaxial compression.

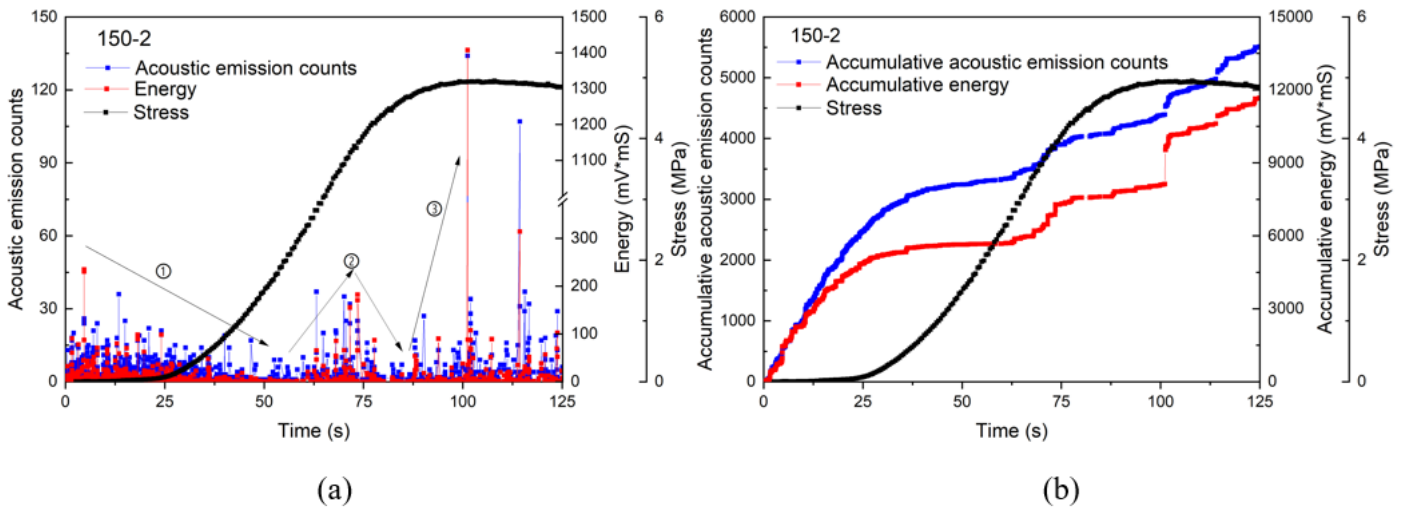


Figure 6

AE characteristics of column cemented gangue backfill body under uniaxial compression.

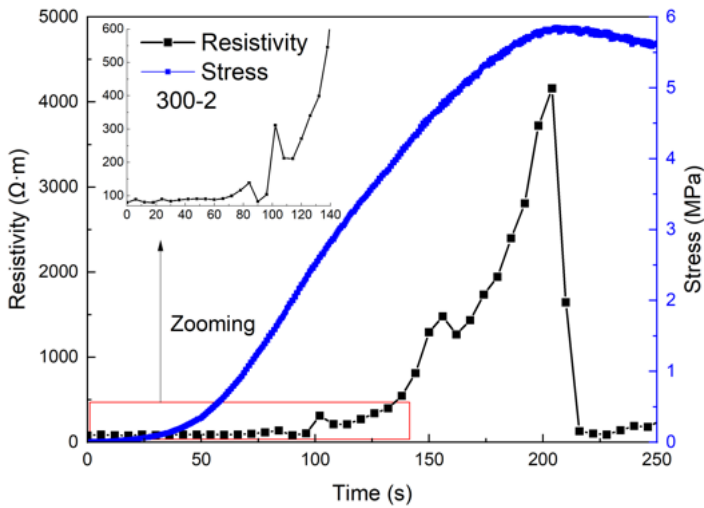


Figure 7

Resistivity-time curve of strip cemented gangue backfill body under uniaxial compression.

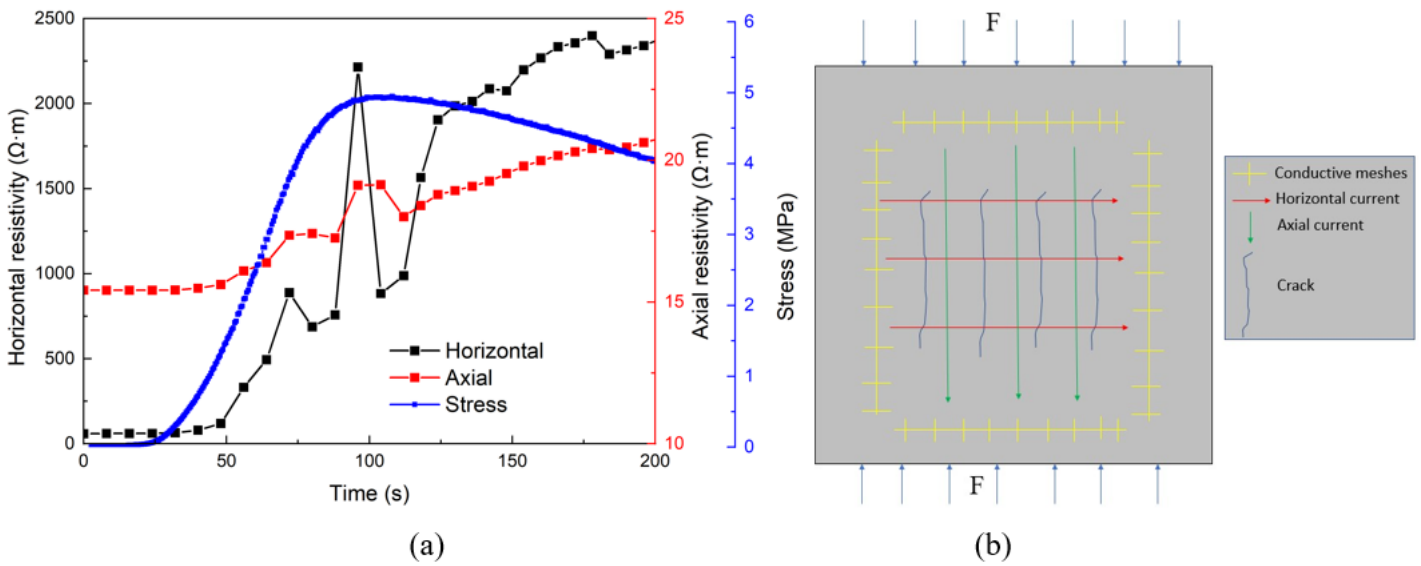


Figure 8

Resistivity-time curve of column cemented gangue backfill body under uniaxial compression.

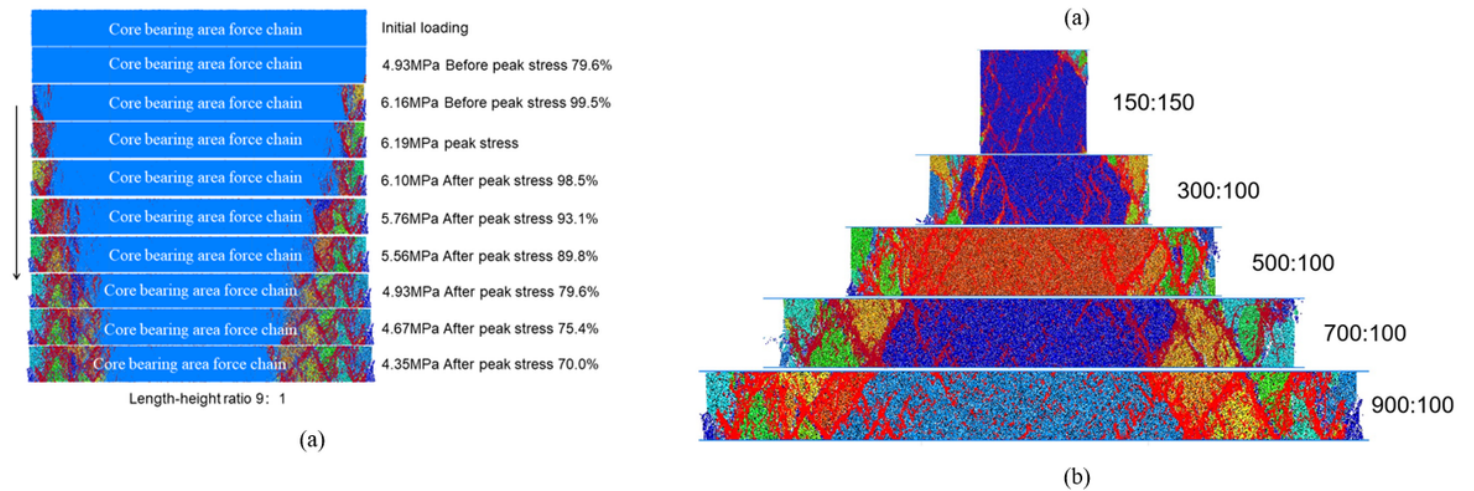


Figure 9

Failure properties of strip cemented gangue backfill body. (a) the crack evolution of the backfill body under uniaxial compression; (b) the crack distribution of the backfill body with the different length-height ratio.

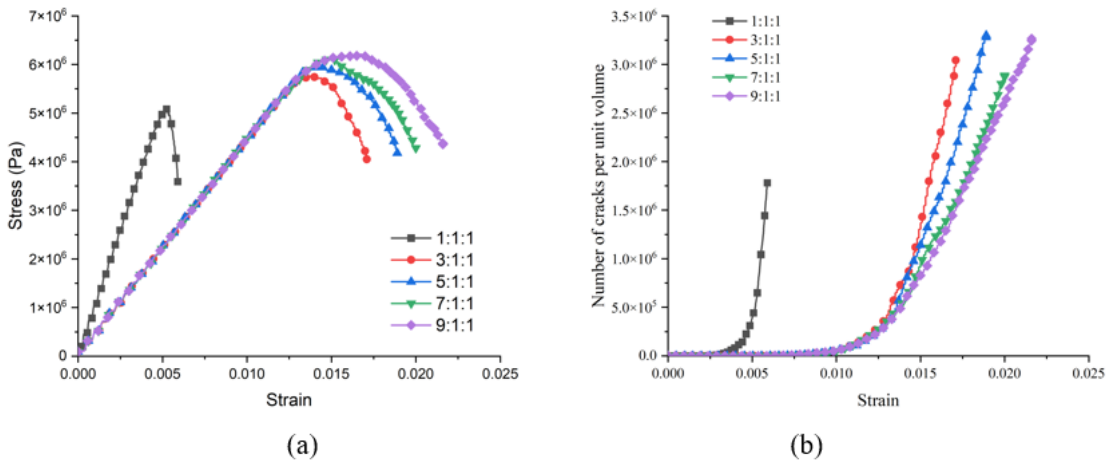


Figure 10

Influence of length-height ratio on the strength of the strip cemented gangue backfill body. (a) the stress-strain curve under different length-height ratios; (b) the number of cracks per unit volume of backfill body with different length-height ratios.

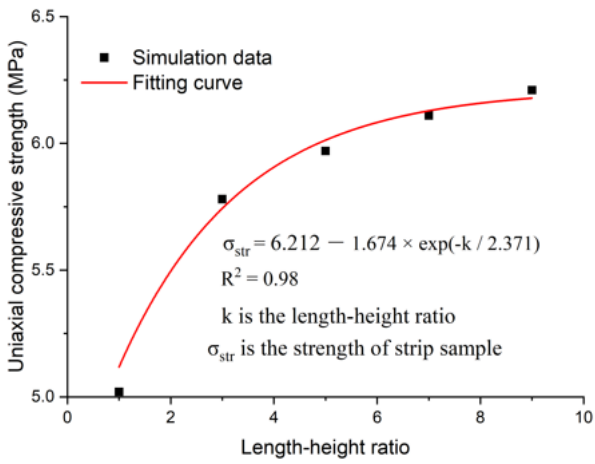
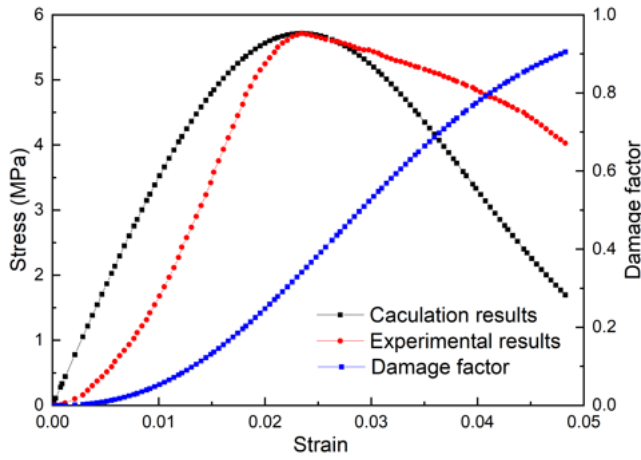
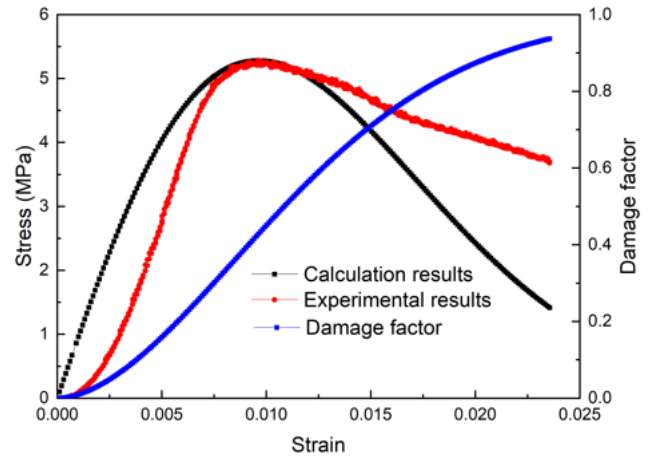


Figure 11

The relationship between length-height ratio and uniaxial compressive strength of strip cemented gangue backfill body.



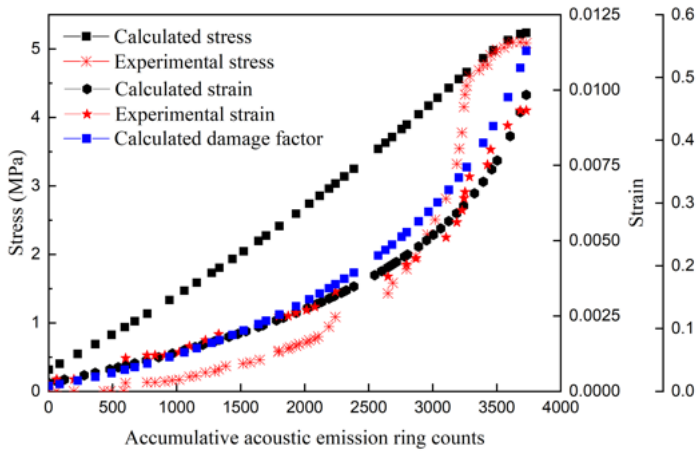
(a) Strip cemented gangue backfill body



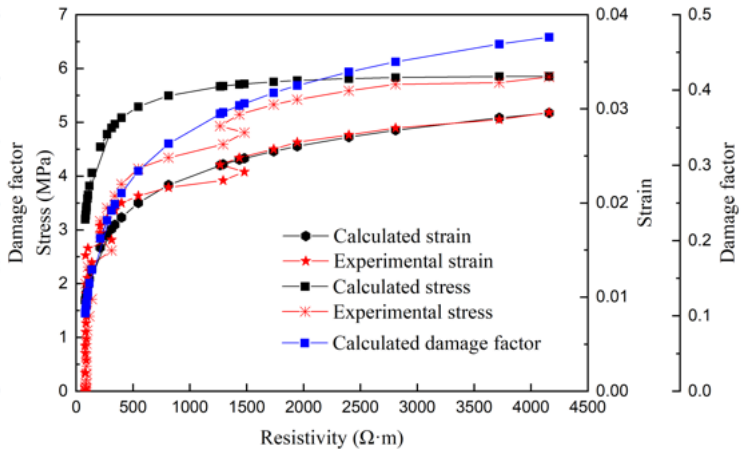
(b) Column cemented gangue backfill body

Figure 12

Experimental and calculation results of damage constitutive model, and the damage factor–strain curve.



(a) Accumulative AE ring counts



(b) Resistivity

Figure 13

Relationship between stress, strain, damage factor, and accumulative acoustic emission ring counts and resistivity.